Hydrogen Bond Network Between Amino Acid Radical Intermediates on the Proton-Coupled Electron Transfer Pathway of E. Coli #2 Ribonucleotide Reductase

JACS
JOURNAL OF THE AMERICAN CHEMICAL SOCIETY
Article
pubs.acs.org/JACS

Hydrogen Bond Network between Amino Acid Radical Intermediates on the Proton-Coupled Electron Transfer Pathway of *E. coli* α2 Ribonucleotide Reductase

Thomas U. Nick,[†] Wankyu Lee,[‡] Simone Koßmann,[§] Frank Neese,*[,§] JoAnne Stubbe,*[,‡] and Marina Bennati*[,†,∥]

[†]Max Planck Institute for Biophysical Chemistry, 37077 Göttingen, Germany
[‡]Department of Chemistry, Massachusetts Institute of Technology, Cambridge, Massachusetts 02139, United States
[§]Max Planck Institute for Chemical Energy Conversion, 45470 Mülheim an der Ruhr, Germany
[∥]Department of Chemistry, University of Göttingen, 37077 Göttingen, Germany

Supporting Information

ABSTRACT: Ribonucleotide reductases (RNRs) catalyze the conversion of ribonucleotides to deoxyribonucleotides in all organisms. In all Class Ia RNRs, initiation of nucleotide diphosphate (NDP) reduction requires a reversible oxidation over 35 Å by a tyrosyl radical (Y_{122}•, *Escherichia coli*) in subunit β of a cysteine (C_{439}) in the active site of subunit α. This radical transfer (RT) occurs by a specific pathway involving redox active tyrosines ($Y_{122} \leftrightarrows Y_{356}$ in β to $Y_{731} \leftrightarrows Y_{730} \leftrightarrows C_{439}$ in α); each oxidation necessitates loss of a proton coupled to loss of an electron (PCET). To study these steps, 3-aminotyrosine was site-specifically incorporated in place of Y_{356}-β, Y_{731}- and Y_{730}-α, and each protein was incubated with the appropriate second subunit $\beta(\alpha)$, CDP and effector ATP to trap an amino tyrosyl radical (NH_2Y•) in the active $\alpha2\beta2$ complex. High-frequency (263 GHz) pulse electron paramagnetic resonance (EPR) of the NH_2Y•s reported the g_x values with unprecedented resolution and revealed strong electrostatic effects caused by the protein environment. ^{2}H electron−nuclear double resonance (ENDOR) spectroscopy accompanied by quantum chemical calculations provided spectroscopic evidence for hydrogen bond interactions at the radical sites, i.e., two exchangeable H bonds to NH_2Y_{730}•, one to NH_2Y_{731}• and none to NH_2Y_{356}•. Similar experiments with double mutants α-NH_2Y_{730}/C_{439}A and α-NH_2Y_{731}/Y_{730}F allowed assignment of the H bonding partner(s) to a pathway residue(s) providing direct evidence for colinear PCET within α. The implications of these observations for the PCET process within α and at the interface are discussed.

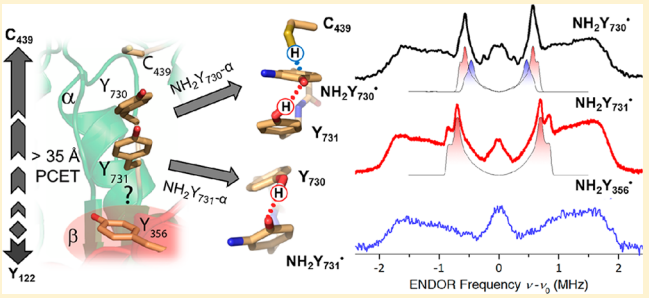

INTRODUCTION

Ribonucleotide reductases (RNRs) catalyze the conversion of four nucleotides (CDP, UDP, ADP, GDP; NDPs) into the corresponding deoxynucleotides (dNDPs).[1,2] Class Ia RNRs are found in nearly all eukaryotic and some prokaryotic organisms[3] and are composed of two homodimeric subunits, $\alpha2$ and $\beta2$, which form an active, transient $\alpha2\beta2$ complex.[4] Subunit $\alpha2$ houses the catalytic substrate binding site and the binding sites for the allosteric effectors that govern specificity and activity of nucleotide diphosphate (NDP) reduction.[5−7] Subunit $\beta2$ houses the diferric-tyrosyl radical cofactor (the Fe^{III}_2-Y•) essential for initiating NDP reduction. During each turnover, the Fe^{III}_2-Y•-$\beta2$ oxidizes C_{439} in the active site of $\alpha2$ where dNDP is produced, and then it is subsequently reoxidized. The oxidation occurs via a radical hopping mechanism over 35 Å between the two subunits along a specific pathway comprised of redox active amino acids ($Y_{122} \leftrightarrows [W_{48}?] \leftrightarrows Y_{356}$ in $\beta2 \leftrightarrows Y_{731} \leftrightarrows Y_{730} \leftrightarrows C_{439}$ in $\alpha2$). Reversible oxidation and reduction of Y during turnover requires release of the phenolic proton to an acceptor concomitant with the oxidation (Figure 1A), a mechanistic strategy to avoid formation of high-energy intermediates.[8] While the long-range oxidation through aromatic amino acid residues in ribonucleotide reductase (RNR) is unprecedented in biology,[4,8,9] proton-coupled electron transfer (PCET) mechanisms are involved in many fundamental processes in biology including photosynthesis, respiration and nitrogen fixation.[10,11] RNRs can thus serve as a paradigm for understanding PCET in a complex biological machine and, in comparison with other systems, offer the opportunity to identify common principles that control this basic transformation. Since PCET is intrinsically of quantum mechanical nature because of both electron and proton tunnels, the large difference in mass (factor ~2000) causes the proton translocation to be limited to very short distances (<1 Å),[8] while the electron may transfer over

Received: October 13, 2014
Published: December 16, 2014

DOI: 10.1021/ja510513z
J. Am. Chem. Soc. 2015, 137, 289−298

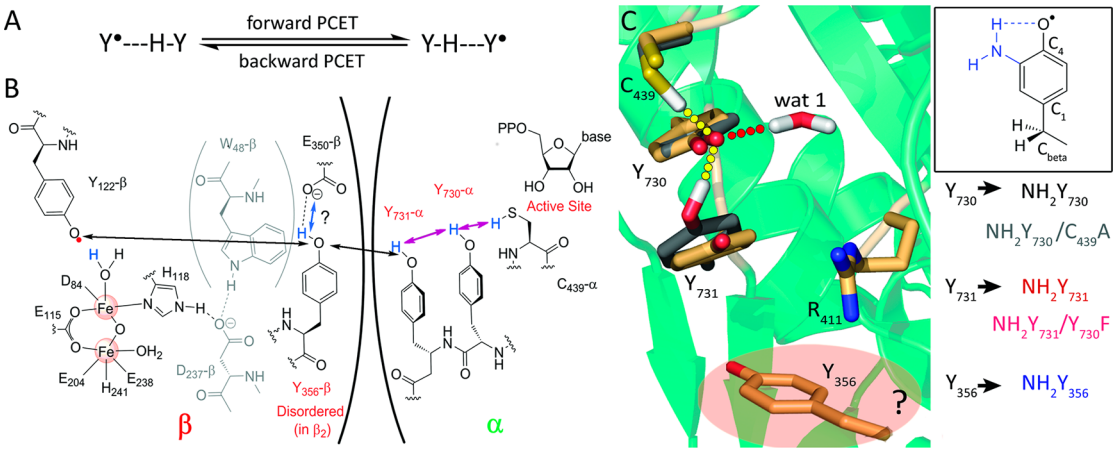

Figure 1. Working model for PCET in *E. coli* RNR. (A) Scheme for concerted PCET between pathway tyrosines within α. (B) Amino acids as well as protons (blue) proposed to be involved in radical transfer between the β and α subunits. W_{48} and D_{237} are shown in gray because there is currently no evidence for their participation in PCET. In β, the protons are proposed to move orthogonal to the electrons (blue vs black arrows) and within α they are proposed to move colinear with the electrons (purple arrows). (C) Overlay of residues in α from the resting state X-ray structure (PDB 2X0X gold/green) with the density functional theory (DFT) optimized structure for radical state Y_{730}• (residues Y_{731}, Y_{730}• and C_{439} in gray shade).[25] Position of the conserved water molecule wat1 as well as on-pathway (yellow dots) and other (red dots) hydrogen bonds are from the DFT structure. The H bond distance of Y_{731} to Y_{730}• is $R_{O730-O731} \sim 2.6$ Å whereas the H bond distances of C_{439} and wat1 to Y_{730}• are $R_{S439-O730} \sim 3.3$ and $R_{Owat1-O730} \sim 2.8$ Å respectively.[25] Location of Y_{356} at the interface between the subunits is unknown. Inset: Chemical structure of NH_2Y• and Ys in the pathway replaced by NH_2Y as well as the double mutants employed in this study.

very long distances. Thus, in PCET the electron and the proton might be transferred to different acceptors (orthogonal or bidirectional) or they might move between the same donor/acceptor pairs (colinear). Description of the coordination of these events has been theoretically challenging and is summarized in recent reviews.[10,12] Investigation of the electron and proton pathways has required RNRs with site-specifically incorporated unnatural amino acids and electron paramagnetic resonance (EPR) combined with electron−nuclear double resonance (ENDOR) spectroscopies have provided a unique opportunity to access mechanistic details if the intermediate radicals can be detected.

The current model for this long-range oxidation is shown in Figure 1B. It was originally proposed based on the X-ray structures of α2 and β2,[13−16] a docking model of these subunits based on their shape complementarity,[15] and conserved residues.[17−20] Recent biophysical studies including pulsed electron−electron double resonance (PELDOR) studies[21,22] and small-angle X-ray scattering studies (SAXS)[6] and cryoEM[23] have established that the docking model is a reasonable representation of the "active" RNR structure in solution and that the oxidation occurs over >35 Å. Unfortunately there is little information about the molecular details of the interface between β and α, more specifically, the communication between Y_{356} in β2 and Y_{731} in α2. The last 25−30 amino acids of all β2 structures which include Y_{356} or its equivalent are structurally disordered and the last 15 amino acids of *Escherichia coli* β2 are largely responsible for the weak interaction between the subunits (K_d of ∼0.1 to 0.2 μM).[17,24]

Studies of this unprecedented oxidation catalyzed by wt RNR have not been possible as protein conformational change(s) constitute the rate-limiting step(s) and kinetically mask *all* of the detailed chemistry of the radical transfer (RT) and the nucleotide reduction step.[26] However, use of technology in which the pathway tyrosines are replaced site-specifically with tyrosine analogues with altered pKas and reduction potentials,[4] and the development of high frequency (HF) EPR[27,28] and ENDOR methods[25] to characterize Y• analogues generated with the mutant RNRs, are now unmasking the chemistry of this long-range oxidation. These studies taken together suggest that conformational gating is occurring within β and that radical intermediates formed at Y_{356}, Y_{731}, Y_{730}, C_{439} and substrate radical are likely in equilibrium along the pathway.[29,30] Their relative redox potentials are progressively uphill with corresponding lower concentrations. However, there is sufficient concentration of the most uphill radical (substrate radical) to drive the reaction to the right by a rapid, irreversible step proposed to be the loss of water during nucleotide reduction. Once the chemical reaction is complete, the reformation of the Y_{122}• in β is energetically downhill.[4]

The results from the incorporation of NH_2Y site-specifically at 356-β, 731- and 730-α, the focus of this paper, have played a critical role in our current understanding of specific steps of the RT pathway and the conformational gating process. In all three cases, NH_2Y•-$\beta(\alpha)$ is generated in ∼30−40% yield upon incubation of the second subunit $\alpha(\beta)$, substrate CDP and allosteric effector ATP.[22,31,32] The formation of the NH_2Y• is a biphasic process with both phases kinetically competent in nucleotide reduction at 5 to 10% the rate of the wt-RNR.[31,32] Three recent experiments using this probe address the importance of PCET and the α2β2 conformational changes triggered by binding substrate and effector. Insight into the initial RT event within β has been studied by rapid freeze quench (RFQ) Mössbauer analysis using wt-β2/NH_2Y_{730}-α2/CDP/ATP.[33] The results established that the proton of the water bound to Fe1 (Figure 1B) is transferred to Y_{122}• coupled with an electron, likely from Y_{356}. Using the NH_2Y_{730}-α2 only the forward radical step is observed and interestingly the Fe1-OH now remains. These results support the model of orthogonal PCET in β2 and the exquisite control dependent on the proton's location (Figure 1B).

Using the same experimental design, analysis of the NH_2Y• by HF EPR and deuterium (^{2}H) ENDOR provided the first spectroscopic insight suggesting the importance of colinear PCET within α2 and the structural relationship of Y_{731} and Y_{730} in the active α2β2 RNR complex.[25] The link between EPR data

DOI: 10.1021/ja510513z
J. Am. Chem. Soc. 2015, 137, 289−298

in the *active* intermediate state and the X-ray structural data in the inactive state was supported by quantum chemical calculations of the energy optimized structural models of Y_{730}•-α and NH_2Y_{730}•-α including 211atoms (Figure 1C). The ENDOR analysis in conjunction with density functional theory (DFT) calculations revealed one strong ($R_{O-O} \sim 2.7$ Å) and one weaker ($R_{S-O} \sim 3.4$ Å) H bond proposed to be associated with residues adjacent to NH_2Y_{730}• in the pathway, as well as another weak ($R_{O-O} \sim 3.0$ Å) interaction with water. The water molecule was proposed to tune the RT rates in wt enzyme around Y_{730} by about 1 order of magnitude.[25] Finally, our recent SAXS and pull-down experiments of RNR from this reaction mixture established that a single H atom transfer from NH_2Y_{730} to Y_{122}• is sufficient to increase the weak α/β subunit affinity by a factor of 10^5.[23] This result again highlights the importance and subtlety of conformational changes in the RT process.

In the current paper, experiments in which NH_2Y has been site specifically incorporated at NH_2Y_{356}-β, and at NH_2Y_{731} and NH_2Y_{730}-α (Figure 1C) in conjunction with HF EPR and HF ^{2}H ENDOR spectroscopies, density functional theory (DFT) calculations using $NH_2Y_{731(730)}$-α structures, have been employed in an effort to understand the electrostatic and H bonding environment at these residues in the RT pathway. HF EPR data were recorded at a microwave frequency of 263 GHz, which delivers unprecedented resolution in the spectra of the NH_2Y•s. In addition, double mutants $NH_2Y_{730}/C_{439}A$-α and $NH_2Y_{731}/Y_{730}F$-α were prepared and the ^{2}H ENDOR results compared to the single mutant results in an effort to assign the source of the H bonds observed to specific residues. Our results support the colinear concerted PCET model within α and provide spectroscopic evidence for the unusual stacking of Y_{730}/Y_{731} in the active $\alpha 2\beta 2$ complex.

RESULTS

Electrostatics and Hydrogen Bond Interactions around the Radical Intermediates. To probe the electrostatic environment of the radical intermediates at the three different positions in the RT pathway we examined the HF EPR spectra formed after incubation of β-NH_2Y_{356}, α-NH_2Y_{731}, α-NH_2Y_{730} with their respective complementary wt subunits, either α or β, CDP, and ATP (Methods). Figure 2 presents 263-GHz pulse EPR spectra from the individually trapped NH_2Y•s recorded with a prototype quasi-optical EPR spectrometer (Methods). The buffer was exchanged with D_2O to enhance EPR resolution. At this frequency, all g_x values of NH_2Y•s (ND_2Y•s) are clearly resolved and shifted by about 1 ppt (or 0.001) from the value calculated for a free NH_2Y• ($g_{x,free} = 2.0061$). This shift is significant, on the order of the effect predicted from several hydrogen bonds.[25,34,35] g values were calibrated with the spectrum of the stable radical Y_{122}• in $\beta 2$, which is present in all samples and visible only at low temperatures. Additionally, g_x slightly decreases starting from the most buried intermediate NH_2Y_{730}• ($g_x = 2.0054$) to NH_2Y_{356}• ($g_x = 2.0049$) located at the subunit interface. As a control, spectra were also recorded in protonated buffer and the g values were best reproduced (Supporting Information, Figure S1). Simulations of the 263 GHz spectra combined with 94 GHz spectra (the latter frequency was used to constrain the simulation, Figure S2) led to a consistent set of g values and C-β proton hyperfine (hf) couplings (see chemical structure in Figure 1 inset) that are summarized in Table 1. Thus, the EPR spectra of the single mutants in the *active* enzyme are contributed by a radical species (per mutant) with a well-defined microenvironment (g value) and molecular orientation. This finding underlines the importance of a specific structural arrangement in the active state to permit radical propagation.

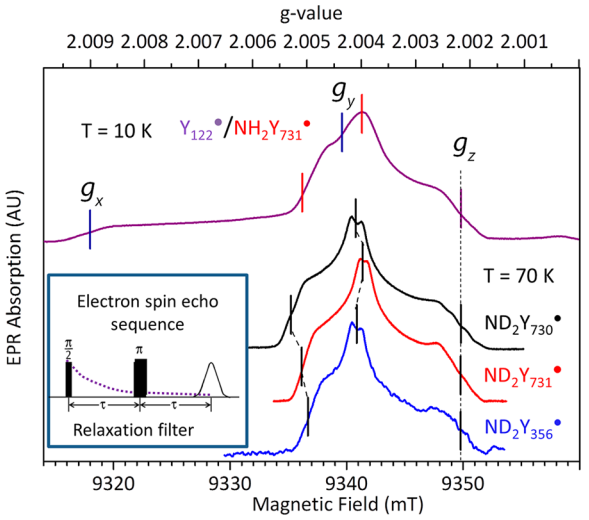

Figure 2. 263-GHz pulse EPR spectra of different NH_2Y•s intermediates. Electron spin−echo (ESE) detected spectra of intermediates without (top spectrum for NH_2Y_{731}•/Y_{122}•, 10 K) and with relaxation filtering (bottom spectra for NH_2Y•s, 70 K). The spin−echo sequence used to suppress the signal of Y_{122}• (box) is based on differences in the transverse relaxation times (T_2) of the radicals: NH_2Y•s and Y_{122}•. At T = 70 K, the signal associated with the Y_{122}• decays during the acquisition (box, purple dotted line) and does not contribute to the spin echo signal. ESE detected EPR spectra of the NH_2Y•s radicals in H/D exchanged buffer: ND_2Y_{730}• (black), ND_2Y_{731}• (red) and ND_2Y_{356}• (blue). Experimental conditions: ESE ($\pi/2-\tau-\pi$−echo) spectra: $\pi/2$ = 60−110 ns, τ = 290 ns, 250−500 averages/point, acquisition time/spectrum =1.5−3 days, T = 10 and 70 K.

Table 1. Summary of g Values and C-β hf Couplings of NH_2Y• at Residues 730, 731, 356[a]

	g_x	g_y	g_z	A_{iso} (C-β)
Experiment				
NH_2Y_{730}•	2.0054, 2.0052[b]	2.0042	2.0022	29
NH_2Y_{731}•	2.0051	2.0040	2.0022	22
NH_2Y_{356}•	2.0049	2.0041	2.0021	27
NH_2Y_{730}•/$C_{439}A$	2.0056	2.00415	2.0022	34
NH_2Y_{731}•/$Y_{730}F$	2.0055/52	2.0041	2.0023	26
DFT				
NH_2Y_{731}• model 1, with wat1	2.0055	2.0042	2.0022	35
NH_2Y_{731}• model 2, no water	2.0050	2.0040	2.0023	28
NH_2Y_{731}• model 3, with wat1 and wat2	2.0051	2.0039	2.0021	22
free NH_2Y•[c]	2.0061	2.0045	2.0022	–

[a]The values were obtained from combined simulations of the 263 and 94 GHz spectra and compared with those obtained from DFT calculations. The ^{14}N hyperfine tensor of the NH_2Y• was not varied in the simulations and kept A_x = 2.4 MHz, A_y = 1.6-5 MHz, A_z = 30.7 MHz.[28] Hf values are in MHz. Uncertainty in g values is about 0.05 ppt for the experiments and 0.5 ppt for DFT calculations. Uncertainty in hf couplings is up to 10% from spectral simulations and up to 20% in DFT calculations. [b]Value reported in ref 28. [c]Value from 2-amino-4-methyl-phenol radical.[25]

DOI: 10.1021/ja510513z
J. Am. Chem. Soc. 2015, 137, 289−298

The observed shift of g_x values is a hallmark for a substantial effect of either positive charges and/or hydrogen bond interactions. Since hydrogen bonds are expected to have a predominant effect on g values,[35] a possible correlation of the observed g_x shifts with the number and strength of hydrogen bonds was examined.

Hydrogen Bonds between On-Pathway Amino Acids. We probed exchangeable hydrogen bonds around the trapped $NH_2Y\bullet$ intermediates by ENDOR spectroscopy at 94 GHz. ENDOR reveals the spectrum of magnetic nuclei that are in the coordination sphere (usually ≤5 Å) of the observed radical. After buffer exchange, exchangeable protons are substituted by deuterons (abbreviated D, with the nucleus denoted ^{2}H), which become visible by ENDOR in the ^{2}H resonance region. Figure 3A illustrates the ^{2}H Mims ENDOR[36] spectra of the three $NH_2Y\bullet$ intermediates ($ND_2Y\bullet$) trapped under comparable conditions as in the EPR experiments. The spectrum of $ND_2Y_{730}\bullet$ was initially reported in ref 25, and it is included here for further analysis. All three spectra contain a broad, almost featureless background extending over ±2 MHz, which arises from the strongly coupled amino deuterons. Additionally, two samples, $ND_2Y_{730}\bullet$ and $ND_2Y_{731}\bullet$, show pairs of sharp peaks in the region ≤1 MHz that is usually dominated by deuterons in the hydrogen bond range (Figure 3A, peaks marked in red and blue). The spectra of $ND_2Y_{730}\bullet$ and $ND_2Y_{731}\bullet$ look quite similar, with the peaks from $ND_2Y_{731}\bullet$ being slightly shifted to larger couplings. The sharp peaks are split by an additional small coupling, i.e., the quadrupol coupling. The ENDOR spectrum can also detect *weak* couplings ($r_{O-H} \geq 2.1$ Å) if they can be resolved from matrix deuterons (matrix line). Indeed, additional small differences are observed here also in the central resonance region (±0.3 MHz). In $ND_2Y_{730}\bullet$, this region was proposed to be associated with a water molecule (wat1, Figure 1) conserved in the structure of wt α2[15,16,37] and ND_2Y_{730}-α2.[32] This resonance pattern is now absent in $ND_2Y_{731}\bullet$ and replaced by a matrix line. Interestingly the spectrum of $ND_2Y_{356}\bullet$ lacks any sharp peaks and is associated with resonances of the amino deuteron and a matrix line.

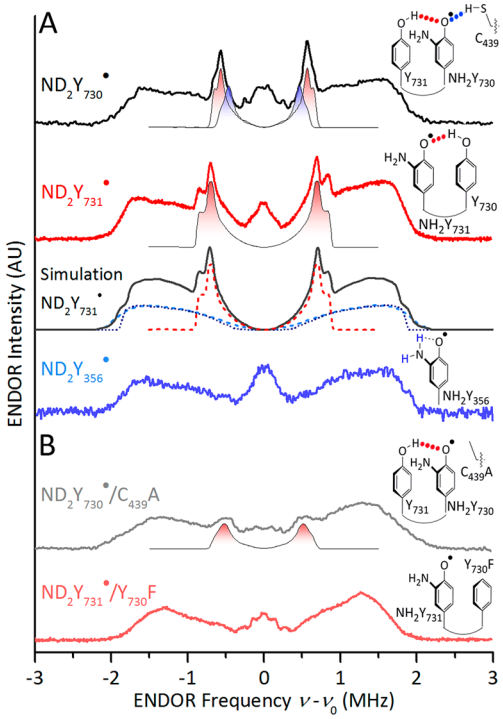

Figure 3. 94-GHz ^{2}H-ENDOR spectra of the trapped $ND_2Y\bullet$ intermediates. (A) Comparison between spectra of $ND_2Y_{730}\bullet$ (black), $ND_2Y_{731}\bullet$ (red), and $ND_2Y_{356}\bullet$ (blue). Simulation of the spectrum for $ND_2Y_{731}\bullet$ (gray) is representatively decomposed into the contributions of the amino deuterons (blue dashed and dotted lines) and of one hydrogen bond (red dashed line). Simulation parameters are reported in Table 2. Spectrum of $ND_2Y_{730}\bullet$ is contributed by one strong (red peaks) and one moderate (blue peaks) H bond.[25] (B) Spectra of double mutants $ND_2Y_{730}\bullet/C_{439}A$ and $ND_2Y_{731}\bullet/Y_{730}F$ (gray and red, respectively). Simulation of the spectrum of the retained H bond (red peaks) with parameters reported in Table S2. The contributions from hydrogen bonds, as assigned here, are illustrated on the right. Exp. parameters: Mims ENDOR with $\pi/2$ = 20 ns, τ = 200 ns, shot repetition time = 10 ms, random RF acquisition[38] at 1 shot/point, acquisition time = 24−55 h, T = 70 K. The same relaxation filtering mechanism was used for the ENDOR experiments at 70 K as for the HF EPR spectra (cf. Figure 2 inset). Excitation in the EPR line was at $B_0 \parallel g_y$. ENDOR spectrum is centered at the Larmor frequency ν_0 of ^{2}H, i.e., 21.9 MHz at a field of 3.3 T.

H-Bond to $NH_2Y_{731}\bullet$. Further experimental evidence for the hydrogen bond at $NH_2Y_{731}\bullet$ was derived from orientation selective HF ^{2}H ENDOR spectra recorded at different field positions in the EPR line. Figure 4A shows Mims ENDOR spectra recorded at the canonical orientations $B_0 \parallel g_x$, g_y and g_z within the region of ±1.5 MHz. Powder patterns are still observed at orientations $B_0 \parallel g_x$ and g_z as orientation selection is moderate for the large excitation bandwidth of the pulses (≈ 1.8 mT) as compared to the total EPR line width (≈ 8 mT); however, clear differences in the line shapes are visible. The smallest hf coupling, taken as the center of the sharp peak, is observed at $B_0 \parallel g_z$ and the hf tensor displays a form $|A_z| \geq |A_y| > |A_x|$ (using the definition $|A_x| < |A_y| < |A_z|$). Previous DFT calculations have indicated that such a tensor form is typical for a deuteron directed almost perpendicular to the tyrosine ring plane, as previously reported also for $ND_2Y_{730}\bullet$,[25] and having the smallest component along the H bond. Such a tensor reflects couplings that still contain some contribution from a scalar interaction arising from orbital overlap. In the following, we define hydrogen bonds with these tensor properties as *strong* to *moderate* ($r_{O-H} \sim 1.7-2.0$ Å). The definition used here is consistent with ref 10 but expanded by the definition of *moderate* bonds. Considering that the g_x tensor component lies along the C−O bond and g_y points to the side of the amino group,[25] the Euler angles α, β, γ between hyperfine A and g tensor obtained from the simulation (Table 2) are consistent with a hydrogen bond directed almost perpendicular to the plane of the $NH_2Y_{731}\bullet$. The mutual tensor orientation is illustrated in Figure 4, inset. Simulations of the entire ^{2}H ENDOR spectrum with the parameters obtained here additionally indicate that the spectrum of a $ND_2Y_{731}\bullet$ can be well reproduced by the contribution of a single hydrogen bond (Figure 3A) according to the observed intensity ratio of the sharp peaks with respect to the amino deuteron resonances.

Preparation and Characterization of $NH_2Y_{731}/Y_{730}F$- and $NH_2Y_{730}/C_{439}A$-α2. In an effort to assign the H bonding interactions observed with NH_2Y_{731}- and NH_2Y_{730}-α2 by ^{2}H ENDOR, double mutants $NH_2Y_{731}/Y_{730}F$ and $NH_2Y_{730}/C_{439}A$ were generated, in which one of the proposed H bonds was removed. The proteins were expressed, purified to homogeneity and characterized by stopped flow-Vis spectroscopy monitoring the rate of loss of $Y_{122}\bullet$ (410 nm) and rate of formation of the $NH_2Y\bullet$ (320 or 325 nm) in the presence of wt-β2/CDP/ATP, Figure S3. The results are summarized in

DOI: 10.1021/ja510513z
J. Am. Chem. Soc. 2015, 137, 289−298

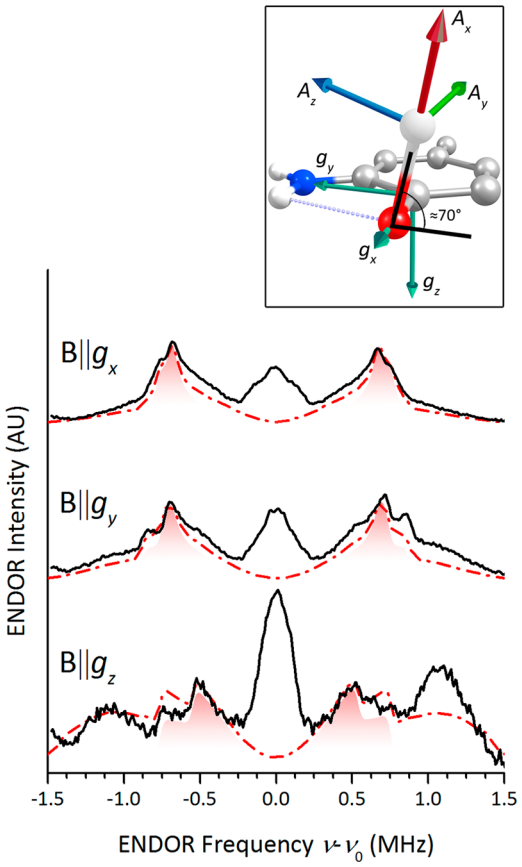

Figure 4. ^{2}H-ENDOR spectra and orientation of the hydrogen bond at NH_2Y_{731}●. ^{2}H 94-GHz Mims ENDOR spectra (black lines) were recorded at field positions in the EPR line parallel to the canonical orientations of the g tensor, i.e., for $B_0 \parallel g_x, g_y, g_z$. Simulations of the spectra (red dashed-dotted curves) were performed as described in the Methods section. Contributions from the hydrogen bond are shown additionally as red peaks. The obtained values are reported in Table 2. A line broadening of 50 kHz was used. Experimental parameters: $\pi/2$ = 20 ns, τ = 320 ns, RF pulse length = 40 μs, shot repetition time = 150 ms, acquisition time = 50 h/spectrum, random RF acquisition,[38] T = 10 K. The low S/N required operation at very low T and contribution of Y_{122}● could not be separated here. However, Y_{122}● does not display any hydrogen bonds but only a matrix line, as also discussed in ref 25. The inset shows the orientation of the ^{2}H hf tensor from the simulation.

Table S1 and compared with results from similar experiments on the single mutants.[32] With NH_2Y_{731}/Y_{730}F-α2, NH_2Y● was formed with biphasic kinetics resulting in 34 ± 3% conversion, similar to the amount formed with NH_2Y_{731}-α2 (32 ± 3%).[32] The kinetics of both phases, however, were slower: 1.5 ± 0.1 and 0.3 ± 0.03 s^{-1} compared to 9.6 ± 0.6 and 0.8 ± 0.1 s^{-1}. Similar studies with NH_2Y_{730}/C_{439}A-α2 resulted in formation of NH_2Y● in only 14 ± 1% conversion, compared with 39% in the single mutant. Furthermore, the rate constant for its formation was decreased ∼10 fold for the double mutant: from 12 ± 1 to 0.13 ± 0.01 s^{-1} and only a single kinetic phase was measured. Attempts to express NH_2Y_{730}/C_{439}S-α2, unfortunately, were unsuccessful. Both double mutants were also characterized by 9 GHz EPR spectroscopy in samples frozen at 30 s (Figure S4). In the case of both double mutants, the altered kinetics of pathway radical formation and its altered amplitude in the case of NH_2Y_{730}/C_{439}A-α2 are likely reflective of the importance of these H bonding interactions in tuning of PCET within α2. To test for possible conformational differences between the NH_2Y● intermediates in the double vs the single mutants, we measured their inter spin distances to the diagonalized Y_{122}● by PELDOR spectroscopy (Figure S5 and S6). The experiments revealed distances of 3.8 and 3.9 nm, respectively, consistent within error (±1 Å) with the distances observed in the single mutants and from the α2β2 docking model in wt; however, the assignment of the 3.9 nm distance in the mutant NH_2Y_{730}/C_{439}A is more uncertain due to the low radical yield and S/N ratio of the PELDOR traces[22] HF EPR spectra (263 GHz) of NH_2Y● trapped in the double mutants also revealed g_x values (Figure S7) different from those in the single mutants, i.e., shifted by +0.3−0.4 ppt in the direction of a free NH_2Y● as expected after removal of a H bond (Table 1).

^{2}H-ENDOR spectra of both double mutants (Figure 3B) display that the sharp peaks at ±0.6−0.7 MHz have dramatically decreased. In the spectrum of NH_2Y_{731}●/Y_{730}F the peaks are now entirely absent, whereas residual peaks (∼30% of initial intensity) are observed in NH_2Y_{730}●/C_{439}A mutant. These results are consistent with the assignment of one H bond to NH_2Y_{731}● associated with Y_{730} and one hydrogen bond to NH_2Y_{730}● associated with C_{439}. Importantly, the spectrum of NH_2Y_{731}●/Y_{730}F gives no evidence for any additional strong H bonds. The NH_2Y_{730}●/C_{439}A mutant, on the other hand, still reveals a contribution of a strong hydrogen bond presumably from Y_{731} as previously proposed by DFT calculations.[25] We note also that the removal of the hydrogen bond is manifested in the hf coupling of the amino deuterons, which slightly decreases as compared to the single mutants due to a change in the spin density distribution on ND_2Y●.

DFT Optimized Structures of α-NH_2Y_{731}●. To obtain a model structure of the radical localized at NH_2Y_{731}●, DFT calculations on representative model systems for NH_2Y_{731}● were performed and the obtained magnetic parameters for g_x and for H bonds were compared with the experimental values. As a starting point, we used the DFT energy optimized structure of Y_{731}● that was previously reported[25] (Methods). Three large models (up to 216 atoms, Figure S8) were considered, which differed by the inclusion of zero, one or two water molecules. The models have taken into account all residues in an interaction sphere of about 5 Å around the oxygen of Y_{731}. The obtained energy-minimized structures are represented in Figure 5.

We found that the presence or absence of the water molecules has an impact on some residues arrangement around NH_2Y_{731}● but not on the formation of a strong H bond with Y_{730}. In optimized models 1 and 2, the distance from the oxygen of NH_2Y_{731}● to the hydrogen of the phenol group of Y_{730} is 1.7 Å. In absence of wat1 (model 2), R_{411} approaches NH_2Y_{731}● with hydrogens from its guanidinium group at distances of 2.1 and 2.6 Å from the oxygen of NH_2Y_{731}●. The calculated g_x values from the two models differ by about 0.5 ppt, with the g_x values of model 2 being closer to the experimental ones (Table 1). In model 3 a second water molecule (wat2) was included as observed in some X-ray structures of wt-α and $NH_2Y_{731/730}$-α (Figure S9) in the vicinity (R_{O-O} ∼ 2.6−3.6 Å) of residue 731. The optimized structure of model 3 finds wat2 within hydrogen bond distance (R_{O-H} ∼1.9 Å) to NH_2Y_{731}●; however, a stronger H bond to the phenoxyl hydrogen of Y_{730} remains (R_{O-H} ∼1.6 Å). The g_x value for the model 3 structure is consistent with the experimental value (Table 1). The computed EPR parameters for the H bond distances and orientations relative to Y_{730} are listed in Table 2.

DOI: 10.1021/ja510513z
J. Am. Chem. Soc. 2015, 137, 289−298

Table 2. Summary of EPR Parameters for the Hydrogen Bond to $NH_2Y_{731}^{\bullet}$[a]

$NH_2Y_{731}^{\bullet}$	A_x [MHz]	A_y [MHz]	A_z [MHz]	α [°]	β [°]	γ [°]	Q_x [MHz]	Q_y [MHz]	Q_z [MHz]
Simulation									
Y_{730}-OD	1.3	−1.43	−1.63	−160	110	80			
				120	40	85	−0.03	−0.09	0.12
ND_2 D(1)	−0.6	−2.9	−3.8	−86	98	90			
				−92	93	−3	−0.04	−0.06	0.11
ND_2 D(2)	0.06	−3.1	−4.2	−96	93	−31			
				−93	84	−121	−0.06	−0.08	0.14
DFT (model 1)									
Y_{730}-OD	1.1	−1.4	−1.7	−164	137	79			
				119	39	85	−0.04	−0.06	0.10
ND_2 D(1)	−0.4	−2.6	−2.8	−86	98	90			
				−92	93	−3	−0.05	−0.07	0.13
ND_2 D(2)	0.04	−2.5	−3.7	−96	93	−31			
				−93	84	−121	−0.06	−0.08	0.14
DFT (model 2)									
Y_{730}-OD	0.75	−1.8	−2.2	−194	147	58			
				−104	121	−88	−0.04	−0.06	0.10
ND_2 D(1)	0.25	−1.4	−1.5	−103	137	95			
				−111	80	12	−0.05	−0.07	0.13
ND_2 D(2)	1.0	−1.0	−1.8	−113	80	−17			
				−76	64	−114	−0.06	−0.08	0.14
DFT (model 3)									
Y_{730}-OD	1.1	−1.7	−2.0	−163	122	81			
				106	25	84	−0.04	−0.06	0.09
ND_2 D(1)	0.47	−2.6	−3.4	−98	99	72			
				−95	80	−15	−0.05	−0.06	0.11
ND_2 D(2)	0.67	−2.63	−3.97	−100	84	−45			
				−98	103	43	−0.05	−0.06	0.11

[a]Parameters were obtained from simulations of the orientation selective 94-GHz ENDOR spectra and comparison with the DFT models. The signs of the couplings from the simulation are only relative to each other within one tensor. The Euler angles (α, β, γ) are defined from the A or Q to the g tensor based on the y convention (positive sign for a rotation is counterclockwise, second rotation is around the y axis). The A and Q (quadrupole) tensor are chosen such that $|A_x| < |A_y| < |A_z|$. Within this definition, for both the amino deuterons and the H bond deuteron the A_x direction results along the bond direction. Euler angles from DFT (in the ORCA output positive rotations are defined clockwise) were transformed into the magnetic resonance convention, for comparison. Uncertainty in the parameters from the DFT and ENDOR simulations is estimated up to about 20%.

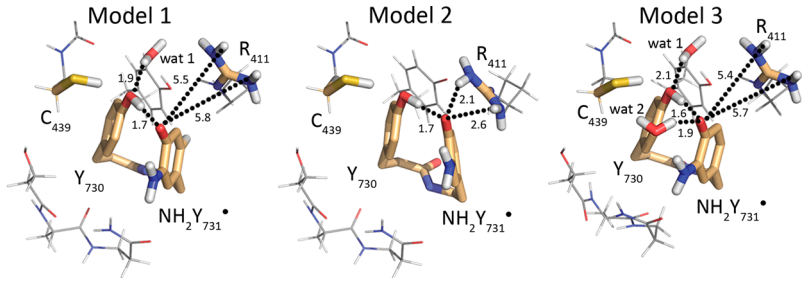

Figure 5. DFT optimized structures of NH_2Y_{731}•. Left: Model 1 includes the water molecule wat1. Center: Model 2 has no water molecules. Model 3 contains a second water molecule wat2, which is observed in some X-ray structures (see text). Residues in interaction distance are in gold. Distances are given in Ångström.

Particularly, all models display an orientation of the strong H bond to NH_2Y_{731}• provided by Y_{730}, which is compatible with the ENDOR data within an uncertainty of about 20% (Table 2, Figure S10).

Considering the accuracy of the calculations, on the order of 0.5 ppt, all three models give g_x values in principle compatible with the experiment. However, considering that the error in the trend of the calculation is smaller than 0.5 ppt, model 2 and 3 better reproduce the experimental g values. The results indicate that the strong g_x shift at NH_2Y_{731}• can be contributed by the combined effect of a strong H bond to Y_{730} and the interaction either to a water molecule (model 3) or alternatively to the positively charged arginine R_{411} (model 2). The findings are further supported by calculations on small model systems (Figure S11), in which the effect of the individual residues R_{411} or Y_{730} was systematically tested. Both scenarios represented in models 2 and 3 find some precedents in the literature. Studies on π−cation interactions revealed that these are common between amino acids like arginine and aromatic amino acids like tyrosine.[39,40] Other studies on small peptides showed that tyrosine/arginine interactions can alter the reduction potential of tyrosines.[41] On the other hand, in PS II two water molecules have been proposed to interact with the redox active Y_Z during PCET and affect their g values.[34] We note that protons of

DOI: 10.1021/ja510513z
J. Am. Chem. Soc. 2015, 137, 289−298

either wat2 or R_{411} possibly located at distances ≥1.9 Å from the phenoxy oxygen might not be resolved in an ENDOR spectrum. Finally we note that the g values for these NH_2Y• can also be affected by the β subunit, which cannot be modeled at present.

DISCUSSION

The electronic and structural features of the NH_2Y•s trapped in the RT pathway of *E. coli* RNR report on how the local protein environment has reorganized after a PCET step to stabilize these intermediates. At each radical state, the protein has rearranged to accommodate a released electron and a proton, a scenario that can be probed by two EPR parameters: the shift in the g_x value caused by positive charges and the hyperfine interaction of protons forming hydrogen bonds of varying strengths. The first parameter is directly accessible from high-frequency EPR spectra[42] but contains only indirect information on hydrogen bond interactions. The second parameter, i.e., the hyperfine coupling to protons exchanged by deuterons, requires ENDOR spectroscopy and much more extensive analysis, which in turn, when attainable, uniquely delivers a high resolution structure of the H bond partners. In this study we report both parameters for the NH_2Y•s trapped within the RT pathway of RNR α subunit. All g_x values of the NH_2Y•s in the three pathway positions are similar and show a considerable shift from the calculated value for a free NH_2Y• (Table 1), consistent with a strongly perturbed electrostatic environment. However, our data reveal that the number, orientation and strength of exchangeable hydrogen bonds at these residues are intrinsically different, reflecting the subtle difference in protein architecture and giving direct insight into the hydrogen bond network involved in PCET.

The ENDOR data display one strong hydrogen bond and one moderate H bond with NH_2Y_{730}• and one strong hydrogen bond with NH_2Y_{731}•. In both cases, the hyperfine couplings and tensor orientations of the two *strong* bonds are very similar (Tables 2 and S2) and indicate that the hydrogen must reside between the two tyrosyl rings (Figures 3 and 4). The direction of the hydrogen bond to NH_2Y_{731}• extracted from the present hyperfine and quadrupole tensors in the ENDOR data (Figure 4) are consistent with the directions predicted by the DFT calculations for a bond with Y_{730} (Figure 5) no matter the number of water molecules considered in the calculation. Moreover, the ENDOR peaks (Figure 3B) of this strong bond disappear when Y_{730} is mutated to F_{730}. These results taken together provide strong evidence for a direct hydrogen bond from Y_{730} to NH_2Y_{731}• and strongly suggest that the proton is directly transferred via colinear PCET, as was proposed by previous quantum chemical calculations.[25,43] Thus, the results support the current model for PCET (Figure 1), that is, that Y_{731}• functions as a proton acceptor for the subsequent RT step to Y_{730}. Moreover, the present DFT calculations provide further insight into this PCET step. They reveal that in each case, the H bond must be directed almost perpendicular to the tyrosyl π system to reproduce the size of the hyperfine tensors and the g_x shift of each NH_2Y•. The results together provide strong support for the π stacking of Y_{731}/Y_{730} in the "active" $\alpha2\beta2$ complex. It should be pointed out that this stacking is observed in some, but not all of the "resting"$\alpha2$ structures (yeast[44] and NH_2Y structures[32] show residue 731 in multiple conformations) and that currently no atomic resolution structural data are available for the complex. The unusual Y/Y π stacking and the implications of this design relative to other configurations for optimum efficiency of transfer has been studied by theorists.[45,46] The work of Kaila and Hummer[45] indicates that this configuration results in strong electronic coupling and adiabatic, colinear PCET, consistent with our data.

Finally, the X-ray structure of the resting states of the wt, NH_2Y_{730}- and NH_2Y_{731}-αs[16,32] and our previous DFT optimized structure of NH_2Y_{730}• and Y_{730}•-$\alpha2$,[25] show that residue C_{439} is in hydrogen bond distance to Y_{730}• (Figure 1C). The present experiments with the double mutant NH_2Y_{730}•/C_{439}A corroborate the assignment of C_{439} as a second moderate hydrogen bond partner of Y_{730}•. Thus, the most direct interpretation of our data combined with the calculated reduction potentials in ref 25. is that residue Y_{730} acts as the direct hydrogen bond acceptor for C_{439}. In principle it still remains possible that water does provide the H-bond, and that the C_{439}A mutant disrupts the H-bonding pattern and eliminates it; however, our experimental data provide no evidence for the participation of a water in this proton transfer step, in contrast to a recent proposal of Bu et al.[47] This group using DFT and QM/MM calculations on several model systems, in which Cys could transfer a proton to Y• including one with the "real protein" environment for C_{439}, Y_{730}•, suggested that the conserved water molecule (H_2O_{138} in their notation is wat1 here) moves and inserts itself between these residues promoting a *double* proton-coupled electron transfer step. However, their calculated barrier for direct PCET between C_{439} and Y_{730}• of 60 kcal/mol is inconsistent with ours[25] and Siegbahn and co-workers[43] calculations, which delivered a barrier of 8−9 kcal/mol. Intriguingly, in one of their model systems with a Cys and Tyr located on different peptide chains[47] mimicking the RNR configuration, the barrier for PCET is almost identical (9 kcal/mol) to our data in the real system.

The studies with NH_2Y_{731}•/Y_{730}F (Figure 3B) failed to reveal a H bonding interaction with a second proton as observed with NH_2Y_{730}•-HSC_{439}. However, in the center of the ^{2}H-ENDOR spectrum, the broad matrix line could be indeed contributed by one or several weak H bonds, which are not resolved. Nevertheless, the DFT calculation revealed that R_{411} is capable of rearranging to form weak hydrogen bonds (≥2.1 Å) if it is not sterically hindered by water molecules, and that this configuration, along with the strong H bond to Y_{730}, can reproduce the observed g_x value. However, a model with two waters (Figure 5), also is capable of recreating the experimentally measured g_x value. The absence of structural insight about the α/β subunit interface and the ability to use the protein environment (R_{411} or two waters) to subtly alter the electrostatic environment, suggests multiple factors contribute to g_x in addition to the strong H bond and our methods cannot currently distinguish between them.

Perhaps the most unexpected observation from the current studies are the results with NH_2Y_{356}•-$\beta2$. In contrast with the pathway residues in $\alpha2$, no exchangeable moderate H bonds to NH_2Y_{356}• are observed outside the matrix line, yet the g_x value is perturbed to a similar extent as those for the NH_2Y•s in $\alpha2$. Our inability to observe crystallographically Y_{356} within $\beta2$ alone or in $\alpha2\beta2$ prevents any specific conclusions about the origin of the g_x shift. However, the data still contribute to our understanding of PCET at this position. For example, one possible mode of communication between Y_{356} and Y_{731} could involve π stacking similar to that observed between Y_{731} and Y_{730}. This type of interaction is unlikely, however, given the

DOI: 10.1021/ja510513z
J. Am. Chem. Soc. 2015, 137, 289−298

absence of any *moderate* H bond. A second possible model of communication for PCET between Y_{356} and Y_{731}, could involve a water molecule or network of water molecules at the subunit interface. The amino protons of NH_2Y_{356}• would likely obscure these weak H bonds as they are adjacent to the matrix line, precluding their detection. The greatly perturbed g_x value of NH_2Y_{356}• in the absence of strong or moderate H bonds requires an altered electrostatic environment provided by the protein. Whether this environment could be provided by water clusters at the interface[48−50] or perhaps by binding of Mg^{2+},[51] long been known to play an important, but still poorly defined role in α/α, α/β and β structure/chemistry,[52] potentially in the interface region of the active complex, requires further analysis.

CONCLUSION

In conclusion, the present data establish a hydrogen bond network between residues 731−730−439 in the α2 subunit. The observed hydrogen bonds and directions provide very strong support for a colinear PCET mechanism, consistent with the recent finding that the turnover rate constants within α are very fast, >14000 s^{-1}, when conformational gating from β is removed by photoinitation.[30] These results differ dramatically from the PCET process at the α/β interface and within β. Our data indicate that colinear PCET and π stacking between Y_{356} and Y_{731} are unlikely, and also reveal the importance of the electrostatic protein environment. Additional spectroscopic experiments could be informative, but structural insight is also essential. Within α2 the combination of protein engineering, spectroscopic data, and quantum chemical calculations has provided much insight into the PCET process within this subunit. Nature appears to have utilized multiple PCET strategies to achieve this long-range oxidation over 35 Å.

METHODS

Sample Preparation. 4-(2-Hydroxyethyl)-1-piperazineethanesulfonic acid (Hepes) was purchased from EMD Bioscience. Adenosine-5′-triphosphate (ATP), cytidine-5′-diphosphate (CDP), reduced β-nicotinamide adenine dinucleotide phosphate (NADPH), hydroxyurea (HU), kanamycin (Km), chloramphenicol (*Cm*), 2XYT media, M9 minimal Salts, L-arabinose (ara), β-mercaptoethanol (β-ME), streptomycin sulfate and NH_2Y were purchased from Sigma-Aldrich. Isopropyl-β-D-thiogalactopyranoside (IPTG) and 1,4-dithiothreotol (DTT) were purchased from Promega. Tris(2-carboxyethyl)-phosphine (TCEP) hydrochloride was purchased from Thermo Scientific. Nucleotide primers were purchased from Invitrogen and *Pfu* Ultra II polymerase was purchased from Stratagene.

$(His)_6$-wt-α2 (2200 nmol/min/mg) and wt-β2 (7000 nmol/min/mg and 1.2 Y• /β2 were expressed and purified by standard protocols.[32,53,54] All α2 mutants were prereduced with 30 mM DTT and 15 mM HU before use.[26] *E. coli* thioredoxin (TR, 40 U/mg) and thioredoxin reductase (TRR, 1800 U/mg) used in assays were isolated as previously described.[55,56] $(His)_6$-NH_2Y_{730}-α2 and $(His)_6$-NH_2Y_{731}-α2 were purified as previously described.[32]

Site-Directed Mutagenesis to Generate $Y_{731}F/NH_2Y_{730}$, $C_{439}A(S)/NH_2Y_{731}$-α2. The Quikchange kit (Stratagene) was used according to manufacturer's protocol to generate each mutant. The template pET-*nrdA* with the appropriate stop codon was amplified with primers 1, 2, and 3 and their reverse complements were used to insert a TTT (Phe) at position 730; GCC (Ala) at position 439 and AGC (Ser) at position 439 (Table 3). Sequences were confirmed by the MIT Biopolymers Laboratory. All constructs contain an N-terminal $(His)_6$-tag with a 10 amino acid linker, as described previously.[32]

Expression and Purification of $NH_2Y_{731}/Y_{730}F$-α2 and $Y_{730}NH_2Y/C_{439}A$-α2. Expression and purification of NH_2Y_{730}-α2 followed previous protocols[32] except that the purification buffer (50 mM Tris, 5% glycerol, 1 mM PMSF, pH 7.6) contained 1 mM TCEP. The typical yield of purified protein is ∼6−7 mg/g cell paste.

Table 3. Primers to Generate pET-*nrdA* Mutants

primer	function	forward primer nucleotide sequence 5′−3′
1	$TAT_{730} \rightarrow TTT_{730}$	G GTC AAA ACA CTG TTT TAG CAG AAC ACC CG
2	$TGC_{439} \rightarrow GCC_{439}$	GCT CAG TCT AAC CTG GCC CTG GAG ATA GCC C
3	$TGC_{439} \rightarrow AGC_{439}$	GCT CAG TCT AAC CTG AGC CTG GAG ATA GCC C

Samples for High Field EPR and ENDOR. α-NH_2Y_{730}, α-NH_2Y_{731}, β-NH_2Y_{356} and their double mutants were combined with the corresponding wt(β /α) 1:1 at final complex concentrations of 100−200 μM in D_2O and H_2O assay buffer as previously described.[28,31] The reaction was initiated at 25 °C by adding CDP and ATP with final concentrations of 2 and 6 mM, respectively, and manually freeze quenched after 10−20 s inside the EPR tube with liquid N_2.

High-Frequency Pulsed EPR and ENDOR. Echo-detected EPR spectra at 263 GHz were recorded on a Bruker Elexsys E780 quasi optical spectrometer using a single mode (TE_{011}) cylindrical resonator (Bruker BioSpin) with a typical quality factor of 500−1000. Maximum microwave power coupled to the resonator was about 15 mW. The electron spin echo ($\pi/2-\tau-\pi-\tau$−echo) was recorded with $\pi/2$ pulse lengths of 60−100 ns. The EPR spectrum of Y_{122}• in wt-β was used as a reference (Figure S1) at 250 μM concentration in assay buffer to calibrate magnetic field. Samples for 263 GHz EPR were inserted in capillaries (0.33 OD, Vitrocom CV2033S/Q) in typical volumes of ∼50 nL. Samples for 94 GHz spectroscopy contained typical volumes of 2 μL in 0.9 mm OD capillaries. Samples frozen in liquid nitrogen were loaded into the resonator immersed in liquid nitrogen and then transferred into the precooled EPR cryostat.

94 GHz pulse EPR and ENDOR spectra were recorded on a Bruker E680 W-band spectrometer with 400 mW microwave output power (Bruker Power Upgrade 2). 94 GHz ^{2}H Mims ENDOR[36] ($\pi/2-\tau-\pi/2-$RF$-\pi/2-\tau-$echo) was carried out using random radio frequency irradiation and 40 μs RF pulses produced with a 250 W RF-amplifier (250A250A, Amplifier Research). All displayed ENDOR spectra were normalized to compare with simulations.

Processing and Simulations of EPR Spectra. Spectra were processed by phasing and baseline correction. Derivatives were obtained by fitting every four points with a second order polynomial and differentiating the function in MATLAB (version 7.10).[57] EPR spectra were simulated using EasySpin "pepper"-routine running under MATLAB.[58,59] The parameters were set to the experimental conditions. The line width was set to 3 G with a line broadening contribution of a 1:1 Gaussian to Lorenzian.

Simulations of ENDOR Spectra. 94-GHz ^{2}H ENDOR spectra were simulated by using a MATLAB routine developed in house that is based on a first order Hamiltonian (high field condition) for the hyperfine and quadrupolar interaction. The blind spots produced by the Mims ENDOR sequence were included by multiplying the calculated ENDOR powder pattern with an envelope function given by $I_{ENDOR} = 1 - \cos(2\pi A\tau)$.[60] This is valid for the $I = 1$ nuclei considered here, as all quadrupole couplings are much smaller than the hyperfine values.[61] All simulations could be reproduced with Easyspin "salt"-routine using perturbation theory.[58,59]

DFT Calculations. All calculations have been performed with the ORCA 3.0.0 program package.[62] The initial model structures were based on the large models **7** and **8** used in ref 25 augmented by the amino group at Y_{731}. Geometry optimizations have been performed using the BP86 gradient corrected density functional[63,64] in combination with Ahlrichs' TZVP basis set of triple-ζ quality.[65,66] Grimme's dispersion correction[67,68] has been applied on top of the SCF calculation. The Resolution of the Identity approximation with the corresponding auxiliary basis sets has been employed throughout. Cartesian constraints were imposed on the position C_α of Y_{730}, Y_{731} and C_{439} as well as C_α and C_β of all surrounding residues. Additionally

DOI: 10.1021/ja510513z
J. Am. Chem. Soc. 2015, 137, 289−298

the Cartesian coordinates of the hydrogen atoms in the truncated GPD model replacing the bonds between C4 and C5 of the ribose as well as the bond between C1 of the ribose and the base were kept fixed. The g-values were calculated using the NH_2Tyr-Cα as gauge origin.

The EPR calculations and geometry optimization of the small models were carried out with the B3LYP[64,69,70] hybrid density functional in combination with the RIJCOSX[71] approximation. Here only the dihedral angle of the peptide bond of Y_{730} and Y_{731} was fixed and the Cartesian restrains for all surrounding C_α's were kept. In the small models a solvation model (COSMO[72]) with polarity $\varepsilon = 24$ was used to compensate protein influences. For all DFT/EPR calculations, Barone's EPR-II (IGLO-II for sulfur) basis set of double-ζ quality has been used in combination with the def2-TZVPP/JK auxiliary basis set for all atoms.[73−75] The energy has been converged to 10^{-9} E_h.

■ ASSOCIATED CONTENT

Supporting Information

Simulations of the 263 and 94 GHz EPR spectra (**1**−**2**). Characterization of the double mutants ($Y_{731}NH_2Y/Y_{730}F$-α2 and $Y_{730}NH_2Y/C_{439}A$-α2) by stopped-flow Vis, 9 GHz EPR, PELDOR and HF EPR measurements (**3**−**7**). Full size of the large DFT models (**8**), crystal structures of α displaying water molecules (**9**), hf tensor orientation from ENDOR simulation and DFT models (**10**) and small DFT models (**11**). Coordinates and absolute energies of the DFT optimized models of Figure 5. This material is available free of charge via the Internet at http://pubs.acs.org.

■ AUTHOR INFORMATION

Corresponding Authors

frank.neese@cec.mpg.de
stubbe@mit.edu
marina.bennati@mpibpc.mpg.de

Notes

The authors declare no competing financial interest.

■ ACKNOWLEDGMENTS

We acknowledge T. Argirevic for the assistance with sample preparation and with the EPR spectra in Figure S2 and in Figure 4. We thank I. Bejenke for the $NH_2Y_{730}/C_{439}A$ PELDOR data recorded within a research stage at the MPIbpc as well as Igor Tkach for the help in technical aspects of the high-field EPR spectrometers and discussing the manuscript, Kanchana Ravichandran for reading the manuscript. Financial support from the Max Planck Society, the DFG-SPP 1601 (MB and FN), IRTG 1422 (MB) and NIH GM29595 (JS) is gratefully acknowledged.

■ REFERENCES

(1) Stubbe, J.; van der Donk, W. A. *Chem. Rev.* **1998**, *98*, 705.
(2) Jordan, A.; Reichard, P. *Annu. Rev. Biochem.* **1998**, *67*, 71.
(3) Lundin, D.; Torrents, E.; Poole, A. M.; Sjoberg, B. M. *BMC Genomics* **2009**, *10*, 1471.
(4) Minnihan, E. C.; Nocera, D. G.; Stubbe, J. *Acc. Chem. Res.* **2013**, *46*, 2524.
(5) Reichard, P. *Arch. Biochem. Biophys.* **2002**, *397*, 149.
(6) Ando, N.; Brignole, E. J.; Zimanyi, C. M.; Funk, M. A.; Yokoyama, K.; Asturias, F. J.; Stubbe, J.; Drennan, C. L. *Proc. Natl. Acad. Sci. U. S. A.* **2011**, *108*, 21046.
(7) Hofer, A.; Crona, M.; Logan, D. T.; Sjöberg, B.-M. *Crit. Rev. Biochem. Mol. Biol.* **2012**, *47*, 50.
(8) Reece, S. Y.; Nocera, D. G. *Annu. Rev. Biochem.* **2009**, *78*, 673.
(9) Stubbe, J.; Nocera, D. G.; Yee, C. S.; Chang, M. C. Y. *Chem. Rev.* **2003**, *103*, 2167.
(10) Migliore, A.; Polizzi, N. F.; Therien, M. J.; Beratan, D. N. *Chem. Rev.* **2014**, *114*, 3381.
(11) Hammes-Schiffer, S.; Stuchebrukhov, A. A. *Chem. Rev.* **2010**, *110*, 6939.
(12) Savéant, J.-M. *Annu. Rev. Anal. Chem.* **2014**, *7*, 537.
(13) Nordlund, P.; Sjoberg, B.-M.; Eklund, H. *Nature* **1990**, *345*, 593.
(14) Hogbom, M.; Galander, M.; Andersson, M.; Kolberg, M.; Hofbauer, W.; Lassmann, G.; Nordlund, P.; Lendzian, F. *Proc. Natl. Acad. Sci. U. S. A.* **2003**, *100*, 3209.
(15) Uhlin, U.; Eklund, H. *Nature* **1994**, *370*, 533.
(16) Eriksson, M.; Uhlin, U.; Ramaswamy, S.; Ekberg, M.; Regnström, K.; Sjöberg, B.-M.; Eklund, H. *Structure* **1997**, *5*, 1077.
(17) Climent, I.; Sjoeberg, B. M.; Huang, C. Y. *Biochemistry* **1992**, *31*, 4801.
(18) Ekberg, M.; Sahlin, M.; Eriksson, M.; Sjöberg, B.-M. *J. Biol. Chem.* **1996**, *271*, 20655.
(19) Rova, U.; Goodtzova, K.; Ingemarson, R.; Behravan, G.; Graeslund, A.; Thelander, L. *Biochemistry* **1995**, *34*, 4267.
(20) Rova, U.; Adrait, A.; Pötsch, S.; Gräslund, A.; Thelander, L. *J. Biol. Chem.* **1999**, *274*, 23746.
(21) Bennati, M.; Robblee, J. H.; Mugnaini, V.; Stubbe, J.; Freed, J. H.; Borbat, P. *J. Am. Chem. Soc.* **2005**, *127*, 15014.
(22) Seyedsayamdost, M. R.; Chan, C. T. Y.; Mugnaini, V.; Stubbe, J.; Bennati, M. *J. Am. Chem. Soc.* **2007**, *129*, 15748.
(23) Minnihan, E. C.; Ando, N.; Brignole, E. J.; Olshansky, L.; Chittuluru, J.; Asturias, F. J.; Drennan, C. L.; Nocera, D. G.; Stubbe, J. *Proc. Natl. Acad. Sci. U. S. A.* **2013**, *110*, 3835.
(24) Hassan, A. Q.; Wang, Y. T.; Plate, L.; Stubbe, J. *Biochemistry* **2008**, *47*, 13046.
(25) Argirević, T.; Riplinger, C.; Stubbe, J.; Neese, F.; Bennati, M. *J. Am. Chem. Soc.* **2012**, *134*, 17661.
(26) Ge, J.; Yu, G. X.; Ator, M. A.; Stubbe, J. *Biochemistry* **2003**, *42*, 10071.
(27) Bennati, M.; Prisner, T. F. *Rep. Prog. Phys.* **2005**, *68*, 411.
(28) Seyedsayamdost, M. R.; Argirevic, T.; Minnihan, E. C.; Stubbe, J.; Bennati, M. *J. Am. Chem. Soc.* **2009**, *131*, 15729.
(29) Yokoyama, K.; Smith, A. A.; Corzilius, B.; Griffin, R. G.; Stubbe, J. *J. Am. Chem. Soc.* **2011**, *133*, 18420.
(30) Olshansky, L.; Pizano, A. A.; Wei, Y.; Stubbe, J.; Nocera, D. G. *J. Am. Chem. Soc.* **2014**, *136*, 16210.
(31) Seyedsayamdost, M. R.; Xie, J.; Chan, C. T. Y.; Schultz, P. G.; Stubbe, J. *J. Am. Chem. Soc.* **2007**, *129*, 15060.
(32) Minnihan, E. C.; Seyedsayamdost, M. R.; Uhlin, U.; Stubbe, J. *J. Am. Chem. Soc.* **2011**, *133*, 9430.
(33) Wörsdörfer, B.; Conner, D. A.; Yokoyama, K.; Livada, J.; Seyedsayamdost, M.; Jiang, W.; Silakov, A.; Stubbe, J.; Bollinger, J. M.; Krebs, C. *J. Am. Chem. Soc.* **2013**, *135*, 8585.
(34) Retegan, M.; Cox, N.; Lubitz, W.; Neese, F.; Pantazis, D. A. *Phys. Chem. Chem. Phys.* **2014**, *16*, 11901.
(35) Un, S. *Magn. Reson. Chem.* **2005**, *43*, S229.
(36) Mims, W. B. *Proc. R. Soc. London, Ser. A* **1965**, *283*, 452.
(37) Yokoyama, K.; Uhlin, U.; Stubbe, J. *J. Am. Chem. Soc.* **2010**, *132*, 8385.
(38) Epel, B.; Arieli, D.; Baute, D.; Goldfarb, D. *J. Magn. Reson.* **2003**, *164*, 78.
(39) Gallivan, J. P.; Dougherty, D. A. *Proc. Natl. Acad. Sci. U. S. A.* **1999**, *96*, 9459.
(40) Ma, J. C.; Dougherty, D. A. *Chem. Rev.* **1997**, *97*, 1303.
(41) Sibert, R. S.; Josowicz, M.; Barry, B. A. *ACS Chem. Biol.* **2010**, *5*, 1157.
(42) Stoll, S. In *Electron Paramagnetic Resonance*; The Royal Society of Chemistry: London, 2011; Vol. *22*, p 109ff.
(43) Siegbahn, P. E. M.; Eriksson, L.; Himo, F.; Pavlov, M. *J. Phys. Chem. B* **1998**, *102*, 10622.
(44) Voegtli, W. C.; Ge, J.; Perlstein, D. L.; Stubbe, J.; Rosenzweig, A. C. *Proc. Natl. Acad. Sci. U. S. A.* **2001**, *98*, 10073.
(45) Kaila, V. R. I.; Hummer, G. *J. Am. Chem. Soc.* **2011**, *133*, 19040.
(46) Mayer, J. M.; Hrovat, D. A.; Thomas, J. L.; Borden, W. T. *J. Am. Chem. Soc.* **2002**, *124*, 11142.

DOI: 10.1021/ja510513z
J. Am. Chem. Soc. 2015, 137, 289−298

(47) Chen, X.; Ma, G.; Sun, W.; Dai, H.; Xiao, D.; Zhang, Y.; Qin, X.; Liu, Y.; Bu, Y. *J. Am. Chem. Soc.* **2014**, *136*, 4515.
(48) Bonin, J.; Costentin, C.; Louault, C.; Robert, M.; Savéant, J.-M. *J. Am. Chem. Soc.* **2011**, *133*, 6668.
(49) Bonin, J.; Costentin, C.; Robert, M.; Routier, M.; Savéant, J.-M. *J. Am. Chem. Soc.* **2013**, *135*, 14359.
(50) Witwicki, M.; Jezierska, J.; Ozarowski, A. *Chem. Phys. Lett.* **2009**, *473*, 160.
(51) Witwicki, M.; Jezierska, J. *J. Phys. Chem. B* **2011**, *115*, 3172.
(52) Saleh, L.; Bollinger, J. M. *Biochemistry* **2006**, *45*, 8823.
(53) Salowe, S.; Stubbe, J. *J. Bacteriol.* **1986**, *165*, 363.
(54) Salowe, S.; Ator, M.; Stubbe, J. *Biochemistry* **1987**, *26*, 4173.
(55) Chivers, P. T.; Prehoda, K. E.; Volkman, B. F.; Kim, B.-M.; Markley, J. L.; Raines, R. T. *Biochemistry* **1997**, *36*, 14985.
(56) Russel, M.; Model, P. *J. Bacteriol.* **1985**, *163*, 238.
(57) Savitzky, A.; Golay, M. J. E. *Anal. Chem.* **1964**, *36*, 1627.
(58) Stoll, S.; Britt, R. D. *Phys. Chem. Chem. Phys.* **2009**, *11*, 6614.
(59) Stoll, S.; Schweiger, A. *J. Magn. Reson.* **2006**, *178*, 42.
(60) Schweiger, A. J. G. *Principles of Pulse Electron Paramagnetic Resonance*; Oxford University Press: Oxford, U.K., 2001.
(61) Doan, P. E.; Lees, N. S.; Shanmugam, M.; Hoffman, B. M. *Appl. Magn. Reson.* **2010**, *37*, 763.
(62) Neese, F. *Wiley Interdiscip. Rev.: Comput. Mol. Sci.* **2012**, *2*, 73.
(63) Perdew, J. P. *Phys. Rev. B: Condens. Matter Mater. Phys.* **1986**, *34*, 7406.
(64) Becke, A. D. *Phys. Rev. A: At., Mol., Opt. Phys.* **1988**, *38*, 3098.
(65) Weigend, F.; Ahlrichs, R. *Phys. Chem. Chem. Phys.* **2005**, *7*, 3297.
(66) Schäfer, A.; Huber, C.; Ahlrichs, R. *J. Chem. Phys.* **1994**, *100*, 5829.
(67) Grimme, S.; Antony, J.; Ehrlich, S.; Krieg, H. *J. Chem. Phys.* **2010**, *132*, 154104.
(68) Grimme, S.; Ehrlich, S.; Goerigk, L. *J. Comput. Chem.* **2011**, *32*, 1456.
(69) Lee, C.; Yang, W.; Parr, R. G. *Phys. Rev. B: Condens. Matter Mater. Phys.* **1988**, *37*, 785.
(70) Becke, A. D. *J. Chem. Phys.* **1993**, *98*, 5648.
(71) Neese, F.; Wennmohs, F.; Hansen, A.; Becker, U. *Chem. Phys.* **2009**, *356*, 98.
(72) Klamt, A.; Schüürmann, G. *Perkin Trans. 2* **1993**, 799.
(73) Barone, V. Structure, Magnetic Properties and Reactivities of Open-Shell Species from Density Functional and Self-Consistent Hybrid Methods, in *Recent Advances in Density Functional Methods, Part I*1996; p. 287.
(74) Weigend, F. *Phys. Chem. Chem. Phys.* **2002**, *4*, 4285.
(75) Kutzelnigg, W.; Fleischer, U.; Schindler, M. In *Deuterium and Shift Calculation*; Springer: Berlin Heidelberg, 1991; Vol. *23*, p 165.

DOI: 10.1021/ja510513z
J. Am. Chem. Soc. 2015, 137, 289−298